Multiple-scattering approach to the x-ray-absorption spectra of 3d transition metals

Michihide Kitamura
Department of Applied Physics, Faculty of Engineering, Utsunomiya University, Utsunomiya 321, Japan

Shinji Muramatsu
Department of Electronic Engineering, Faculty of Engineering, Utsunomiya University, Utsunomiya 321, Japan

Chikara Sugiura
Department of Applied Physics, Faculty of Engineering, Utsunomiya University, Utsunomiya 321, Japan
(Received 27 August 1985)

The x-ray-absorption near-edge structure (XANES) has been calculated for the 3d transition metals Cr, Fe, Ni, and Cu from a multiple-scattering approach within the muffin-tin-potential approximation, as a first step to studying the XANES for complicated materials. The muffin-tin potential is constructed via the Mattheiss prescription using the atomic data of Herman and Skillman. It is found that the XANES is sensitive to the potential used and that the calculated XANES spectra reproduce the number of peaks and their separations observed experimentally. The final spectra, including the lifetime-broadening effect, show the general features of each material. We emphasize that the multiple-scattering theory which can be applied to the disordered systems as well as the ordered ones may be promising as a tool to analyze the XANES of complicated materials.

I. INTRODUCTION

The recent development, both theoretical and experimental, of x-ray-absorption spectroscopy is remarkable. It is well known that x-ray-absorption spectra from materials are separated into two parts according to the spectral region. One is the structure ranging from the absorption threshold up to about 50 eV, the so-called x-ray-absorption near-edge structure (XANES) and the other is called extended x-ray-absorption fine structure (EXAFS), which appears in the higher-energy region following the XANES. The reason for such classification consists in the fact that in the energy region for XANES the scattering amplitude $f(\theta)$ of a photoelectron depends weakly on the scattering angle θ, while in the region of EXAFS the scattering is dominated by single backscattering events.[1] Hence, EXAFS can be well explained by single scattering theory. The method for the analysis of EXAFS spectra has been established[2] and is widely used as a tool to extract information about the local geometry of an excited atom, i.e., the distance to and number of atoms in adjacent shells.

The procedures employed so far to calculate x-ray-absorption spectra have been based on one of two approaches: scattering formalism (short range)[3-6] or band-structure calculations (long range).[7-9] In the last several years, the method based on the band-structure calculation has been extensively developed by Müller and co-workers, so as to cover the EXAFS range as well as the XANES one, and successfully applied to computing the K and L absorption spectra for transition metals. On the other hand, the short-range approach was extended to the XANES range by including multiple-scattering (MS) events and applied to a variety of materials involving disordered systems. However, theoretical study of XANES seems to have been less active than that for EXAFS because of the complexity involved in the MS processes. The establishment of a method for an analysis of the XANES spectra as a tool to extract information different from that obtained from EXAFS is highly desired.

In this paper we have calculated the K x-ray-absorption spectra from 3d transition metals (Cr, Fe, Ni, and Cu) using MS theory to explore the possibility of its providing a tool for structural analysis, as well as to get an insight into the nature of the x-ray-absorption process. We have chosen these simple typical metals as a first step to a further study of more complicated systems, such as complex metal compounds, because no report based on the short-range approach has been made for these typical metals, as far as we know.

II. THEORETICAL

Our calculations were carried out following the formulation developed by Fujikawa *et al.*[6] We briefly outline those parts necessary to our calculations and discuss the results obtained. This XANES theory is based on the following assumptions.

(1) A one-electron approximation is adopted.

(2) The x-ray absorption is treated as a single-particle process in the electric-dipole approximation.

(3) The potential by which the photoexcited electron is scattered is assumed to be of the short-range type. In practice, a muffin-tin potential is used.

(4) The scattering is assumed to be elastic.

In the following, atomic units are used (the unit of length is 1 Bohr radius, $a_B = 0.529\,17$ Å; the unit of energy 1 Ry = 13.605 eV).

Let us consider a situation where the incident x ray with an energy ω excites an atom located at the origin denoted by zero in Fig. 1. The photoelectron from the absorbing atom at the origin experiences in general j $(=0,1,2,\ldots)$ scatterings by the surrounding atoms, until it reaches the observation point P at $\mathbf{R}$. According to assumption (3), the wave function $\Psi_{\mathbf{k}}(\mathbf{R})$ for this photoelectron at R $(\rightarrow\infty)$ can be written as

$$\Psi_{\mathbf{k}}(\mathbf{R})\simeq\frac{e^{ikR}}{R}\sum_{j=1}^{\infty}\phi^{j}(\mathbf{k}) , \tag{1a}$$

$$\phi^{0}(\mathbf{k})=\sum_{L}Y_{L}^{*}(\hat{\mathbf{R}})M_{LL_0} , \tag{1b}$$

$$\Delta\phi(\mathbf{k})=\sum_{j=1}^{\infty}\phi^{j}$$

$$=\sum_{\alpha}e^{-i\mathbf{k}\cdot\mathbf{R}_{\alpha}}\sum_{L}\sum_{L'}Y_{L'}^{*}(\hat{\mathbf{R}})[\tilde{T}(1-\tilde{T})^{-1}]_{\alpha L';0L}M_{LL_0'} , \tag{1c}$$

where $\mathbf{k}$ is the wave vector for the photoelectron and its magnitude is related to its energy through $k=E^{1/2}$; $Y_L(\hat{\mathbf{R}})$ is a complex spherical harmonic with the $L=(l,m)$. M_{LL_0} denotes the quantity involving the matrix element for the transition from a core state $|L_0\rangle\equiv f_{l_0}(r)Y_{L_0}(\hat{\mathbf{r}})$ to the final state $|L\rangle\equiv R_l(r)Y_L(\hat{\mathbf{r}})$. Under assumption (2), it takes the form[6,10]

$$M_{LL_0}\propto(-1)i^{-l}e^{i\delta_l^0}\sqrt{\omega}\langle L|z|L_0\rangle , \tag{2}$$

where δ_l^{α} is the phase shift for the lth partial wave due to the potential scattering at atom α. The supermatrix $\tilde{T}$ in (1c), which describes the propagation of the photoelectron between atoms at the α and β sites, has the following components:

$$\{\tilde{T}\}_{\alpha L;\beta L'}=t_l^{\alpha}(k)G_{LL'}(\mathbf{R}_{\alpha}-\mathbf{R}_{\beta})(1-\delta_{\mathbf{R}_{\alpha},\mathbf{R}_{\beta}}) . \tag{3a}$$

Here, $t_l^{\alpha}(k)$ and $G_{L'L}(\mathbf{R})$ are the partial scattering amplitude for the potential scattering at atom α and the angular momentum representation of the free-electron Green function, respectively,

$$t_l^{\alpha}(k)=-(e^{2i\delta_l^{\alpha}}-1)/2ik , \tag{3b}$$

$$G_{L'L}(\mathbf{R})=-4\pi ik\sum_{l''}i^{-l''}(-1)^{l-l'+m'}G(Ll'-m'|l'')\times h_{l''}^{(1)}(kR)Y_{l'',m-m'}^{*}(\hat{\mathbf{R}}) , \tag{3c}$$

where $h_l^{(1)}$ is the spherical Hankel function of the first kind and $G(L_1L_2|L_3)$ is the Gaunt coefficient defined by

$$G(L_1L_2|L_3)\equiv\int d\hat{\mathbf{r}}\,Y_{L_3}^{*}(\hat{\mathbf{r}})Y_{L_1}(\hat{\mathbf{r}})Y_{L_2}(\hat{\mathbf{r}}) . \tag{3d}$$

The geometrical information on the surrounding atoms is contained in $G_{L'L}(\mathbf{R})$.

The scattering cross section σ is given by

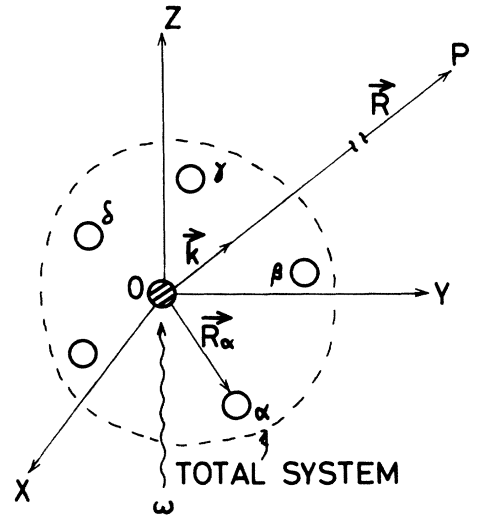

FIG. 1. Schematic diagram illustrating the absorbing atom, its surrounding atoms, and observation point.

$$\sigma=\int d\hat{\mathbf{R}}\left|\sum_{j}\phi^{j}\right|^{2}$$

$$=\int d\hat{\mathbf{R}}\,|\phi^{0}|^{2}+\int d\hat{\mathbf{R}}[2\,\mathrm{Re}(\phi^{0*}\Delta\phi)+|\Delta\phi|^{2}]$$

$$=\sigma_0+\Delta\sigma=\sigma_0(1+\chi) , \tag{4}$$

where the σ_0 given by $\sum_L|M_{LL_0}|^2$ corresponds to the cross section when there is no surrounding atom. χ, defined as $\Delta\sigma/\sigma_0$, represents the modulation of the scattering amplitude due to the presence of the surrounding atoms. Then, the absorption coefficient μ is expressed in terms of χ and the density of states $N(E)\propto E^{1/2}$ for the free electron as follows:

$$\mu\propto\omega^{-1}N(E)\sigma(E)[1-f(E)] \tag{5a}$$

$$\propto\sum_{L}|\langle L|z|L_0\rangle|^{2}E^{1/2}[1+\chi(E)][1-f(E)] , \tag{5b}$$

where $f(E)$ is the Fermi distribution function,

$$\{1+\exp[(E-E_F)/k_BT]\}^{-1} .$$

In Eq. (5b) we have used σ_0 as proportional to ω and the energy is measured from the muffin-tin zero. By using Eqs. (1b) and (1c) and taking L_0 as (0,0), we obtain the final explicit expression for $\chi(E)$ in the case of K absorption,

$$\chi(E)=\chi_1+\chi_2+\chi_3+\chi_4 , \tag{5c}$$

$$\chi_1=2\,\mathrm{Re}\{\mathbf{S}_{0(10)}\} , \tag{5d}$$

$$\chi_2=8\pi\,\mathrm{Re}\left[\sum_{\alpha\neq0}\sum_{L_1L_2}i^{-l_2}j_{l_2}(kR_{\alpha})Y_{L_2}(\hat{\mathbf{R}}_{\alpha})\times G(L_1L_2|10)\mathbf{S}_{\alpha L_1}\right] , \tag{5e}$$

$$\chi_3=\sum_{\alpha}\sum_{L}|\mathbf{S}_{\alpha L}|^2, \tag{5f}$$

$$\chi_4=4\pi\sum_{\alpha\neq\beta}\sum_{L_1L_2L_3} i^{l_3}j_{l_3}(kR_{\alpha\beta})Y_{L_3}(\hat{\mathbf{R}}_{\beta\alpha}) \times G(L_3L_1\,|\,L_2)\mathbf{S}^{*}_{\beta L_2}\mathbf{S}_{\alpha L_1}, \tag{5g}$$

where $\mathbf{R}_{\alpha\beta}=\mathbf{R}_{\beta}-\mathbf{R}_{\alpha}$, and the abbreviated notation $\mathbf{S}_{\alpha L}\equiv[\tilde{T}(1-\tilde{T})^{-1}]_{\alpha L;0(10)}$ is used. The quantity $\sum_L|\langle L\,|\,z\,|\,L_0\rangle|^2$ in Eq. (5b) reduces to $|\langle 10\,|\,z\,|\,00\rangle|^2$.

III. CALCULATION

The first part of the calculation is to obtain the muffin-tin potential from which the logarithmic derivative $R_l'(r)/R_l(r)\,|_{r=r_0}$ $(\equiv L_l)$ is determined, as a function of the energy E (or k), by means of numerical integration for the radial wave function $R_l(r)$ within the muffin-tin sphere. Once the muffin-tin potential is built up and the logarithmic derivative L_l is determined, it is an easy task to compute the scattering phase shift δ_l of the muffin-tin potential which is given by the relation

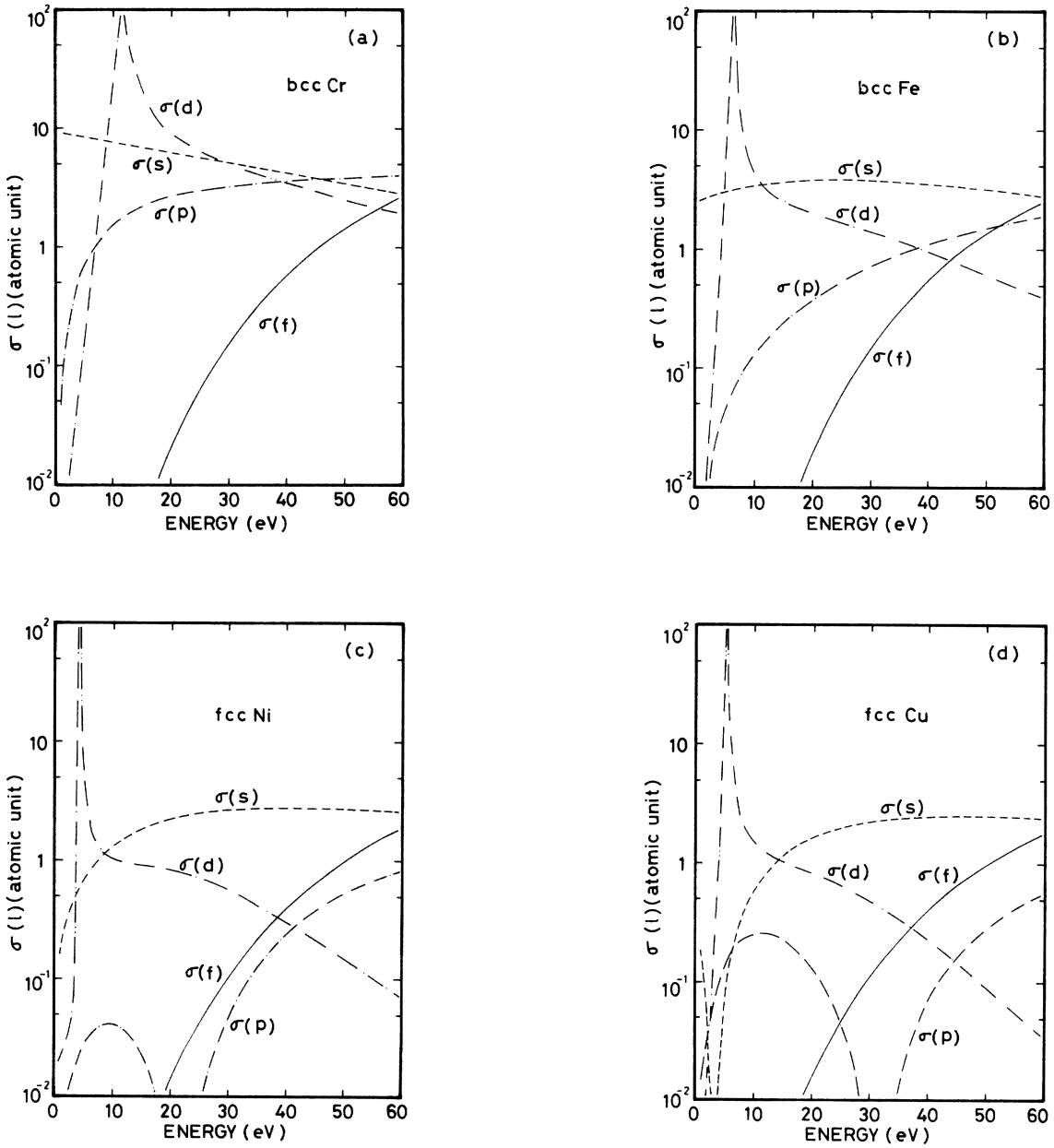

FIG. 2. Energy dependence of the partial-wave scattering cross section $\sigma(l)$ ($l=s$, p, d, and f) for (a) bcc Cr, (b) bcc Fe, (c) fcc Ni, and (d) fcc Cu metals.

$$\delta_l = \tan^{-1}\left[\frac{kj_l'(x)-L_l j_l(x)}{kn_l'(x)-L_l n_l(x)}\right]_{x=kr_0},$$

where j_l and n_l are spherical Bessel and Neuman functions and r_0 is the muffin-tin radius which is taken to be half the minimum interatomic distance a_0. Here, we should note that it is only the scattering phase shift which depends on the muffin-tin potential.

We have constructed the muffin-tin potential using the so-called Mattheiss prescription,[11] which approximates the crystal potential by a superposition of atomic potentials. The atomic potentials were calculated from the atomic data of Herman and Skillman.[12] Numerical calculations after the determination of δ_l are rather straightforward.

In the calculation of $\chi(E)$ in Eq. (5c), the size of the supermatrix $\tilde{T}$ should be truncated at a certain finite size N, which is given by $(l_{\max}+1)^2 N_{\text{atom}}$. Here, N_{atom} is the number of atoms which is taken into consideration. If we take into account the surrounding atoms up to the third shell, $N_{\text{atom}}=43$ in the fcc structure and $N_{\text{atom}}=29$ in the bcc structure. From experience with band-structure calculations for the $3d$ transition metals, it is necessary to take $l_{\max}\geq 2$, where $l_{\max}$ is the maximum value of the order of the expansion in the angular momentum representation for the $\tilde{T}$ matrix. Throughout the present paper, we set the third shell to the maximum size of the cluster ($S_{\max}$), included in the calculations because of the memory area available in the computer and the computation time.

IV. RESULTS AND DISCUSSION

Before proceeding to the calculation of the XANES following Eq. (5), we calculated the matrix element $\langle 10 \mid z \mid 00\rangle$ by using Müller's expression[9] to check the energy dependence of the oscillator strength and found that it does not depend on the energy in the muffin-tin approximation. So we treated it as a constant in our calculations. Furthermore, in order to see the contribution of partial-wave scattering to the XANES, we have calculated these cross sections $\sigma(l)$ ($l=s$, p, d, and f) for the muffin-tin potentials constructed from the atomic data of Herman and Skillman for Cr, Fe, Ni, and Cu. Their results are shown in Fig. 2. It is seen that the $\sigma(f)$ is almost independent of the materials. Since the scattering effect is determined by the value of the scattering cross section, it is expected that the effect of the $\sigma(f)$ mainly appears in the high-energy region.

We have calculated the XANES for bcc Cr and fcc Ni, varying $l_{\max}$ from 2 to 3 and setting the maximum cluster size ($S_{\max}$) to the second or third shell, in order to examine how the XANES depends on $l_{\max}$ and $S_{\max}$. We have chosen the following three cases: $(l_{\max},S_{\max})=(2,2)$, $(l_{\max},S_{\max})=(3,2)$, and $(l_{\max},S_{\max})=(2,3)$.

Furthermore, it is necessary to incorporate the lifetime broadening effect in the result for Eq. (5) to obtain the final result which is compared with the experimental result. We have adopted the procedure used by Müller and Wilkins,[9] that is, convoluted the spectrum obtained from Eq. (5) with a Lorentzian function of the width[8,13] corresponding to finite lifetimes of the initial and final states in the electronic transition. The broadened spectra will be described in Sec. IV D.

TABLE I. The peak separation ΔE in eV for bcc Cr (see Fig. 3).

Spectrum	$\Delta E_{B_1B_2}$	ΔE_{B_2C}	ΔE_{CD_1}
a	7.2	10.0	11.6
b	6.8	9.5	10.4
c	6.3	9.8	12.8
d	7.4	9.2	12.6
Expt.[a]	7.5	8.5	10.5

[a]Reference 14.

A. bcc Cr

Figure 3 shows the calculated spectra of the XANES of bcc Cr along with the experimental result reported by Grunes,[14] and peak separations for both spectra are listed in Table I. From the calculated results *a* and *b* in Fig. 3, it is seen that the contribution of the *f* partial wave to the XANES is only to shift the high-energy peak D_1 to the lower-energy side, as expected from the result of the scattering cross section. The spectrum, shown in curve *c*

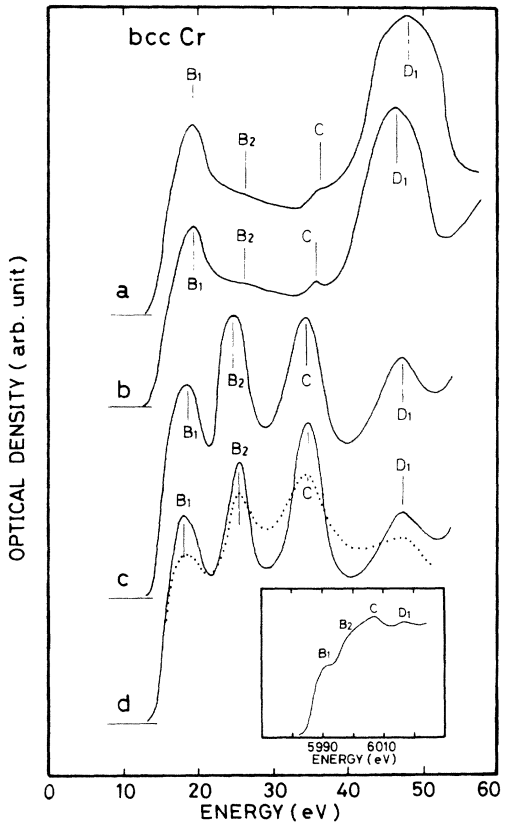

FIG. 3. Calculated *K* XANES spectra for bcc Cr. The experimental spectrum (Ref. 14) is shown in a small framework. The curves *a*, *b*, and *c* are the spectra for the cases of $(l_{\max},S_{\max})=(2,2)$, (3,2), and (2,3), respectively, and *d* denotes the spectrum obtained by setting $r_0=0.9a_0/2$ in the case $(l_{\max},S_{\max})=(2,3)$. In the dotted curve in *d*, the broadening effect is included.

TABLE II. The peak separation ΔE in eV for fcc Ni (see Fig. 4).

Spectrum	$\Delta E_{B_1B_2}$	ΔE_{B_2C}	ΔE_{B_1C}	ΔE_{CD}
a			10.8	9.4
b			12.0	14.8
c	6.2	6.6	12.8	8.0
Expt.[a]	4.0	10.5	14.5	8.2

[a]Reference 14.

TABLE III. The peak separation ΔE in eV for bcc Fe (see Fig. 5).

Spectrum	$\Delta E_{B_1B_2}$	ΔE_{B_2C}	ΔE_{CD}
Calc.	8.6	7.0	13.0
Expt.[a]	8.0	8.0	10.0

[a]Reference 14.

in Fig. 3, which has been obtained by taking into account the surrounding atoms up to the third shell, differs drastically from *a* and *b* in Fig. 3, exhibiting its peak separations in fair agreement with the experiment. If we could perform the calculation in the case of $(l_{\max},S_{\max})=(3,3)$, it would give a better fit to the experimental, since the D_1 peak would be shifted to the lower-energy side by inclusion of the effect of $l=3$.

B. fcc Ni

Figure 4 shows the calculated results together with experimental results[14] for fcc Ni, and Table II tabulates their peak separations. We can see that the $l_{\max}$ dependence appears over a wide range of energy, which is different from the case of the bcc Cr. This behavior is due to the fact that the $\sigma(s)$, $\sigma(p)$, and $\sigma(d)$ of fcc Ni are smaller than those of bcc Cr and that $\sigma(f)$ is of the same order of magnitude as the other cross sections, as shown in Fig. 2. Depending on $S_{\max}$, the XANES shows a large change in the peak intensities, as in the case of bcc Cr. Here, we should point out that a shoulder B_2 appears in the spectrum calculated by setting $(l_{\max},S_{\max})=(2,3)$ and that the profile of this spectrum is similar to the experimental one.

C. bcc Fe and fcc Cu

As discussed in Secs. IV A and IV B, $(l_{\max},S_{\max})=(2,3)$ gives the best result in the two cases. Thus, we calculated the *K* XANES for bcc Fe and fcc Cu under the same conditions. These results are shown in Figs. 5 and 6, and the peak separations are listed in Tables III and IV, where experimental results[14] are also given.

For bcc Fe, the spectrum is similar to that of bcc Cr, except that the B_2 peak is smaller than that of the latter. This is closely related to the similarity of the electronic band structure for materials with the same crystal structure. The peak separation (ΔE_{CD}) of the calculated result is larger than the experiment. It will be improved by the inclusion of the effect of $l=3$. However, the unbroadened profile is poor, because the relative peak intensities are far from the experimental results; in particular, the B_2 peak is smaller than the B_1 peak.

For fcc Cu, whose result is shown in curve *a* in Fig. 6, if we tolerate the shoulder which appears instead of the *B* peak observed experimentally, the overall profile of the calculated spectrum is not far from the experimental one, but its agreement with the experiment is worse than in the case of fcc Ni because the energy separation between the *C* and *D* peaks is considerably smaller than the experimental value. In addition, we have tried to calculate the

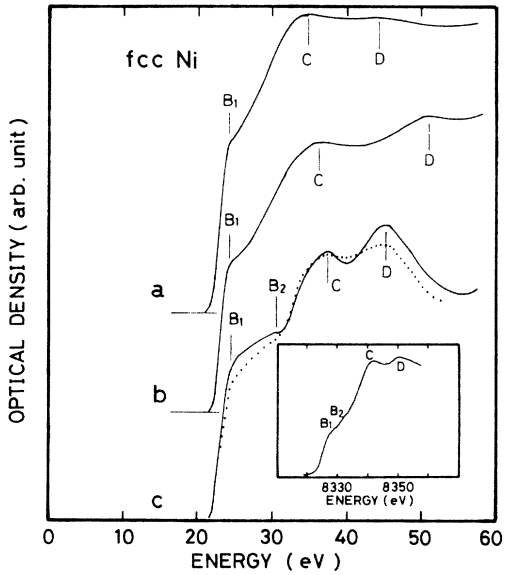

FIG. 4. Calculated *K* XANES and the experimental (Ref. 14) spectra for fcc Ni. The meaning of the curves *a*, *b*, *c*, and the dotted curve is the same as in Fig. 3.

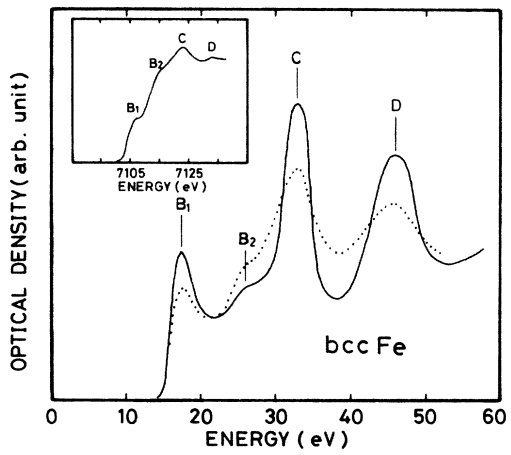

FIG. 5. Calculated *K* XANES spectrum for bcc Fe in the case of $(l_{\max},S_{\max})=(2,3)$ and the experimental (Ref. 14) one. The dotted curve is broadened by the inclusion of the lifetime broadening effect.

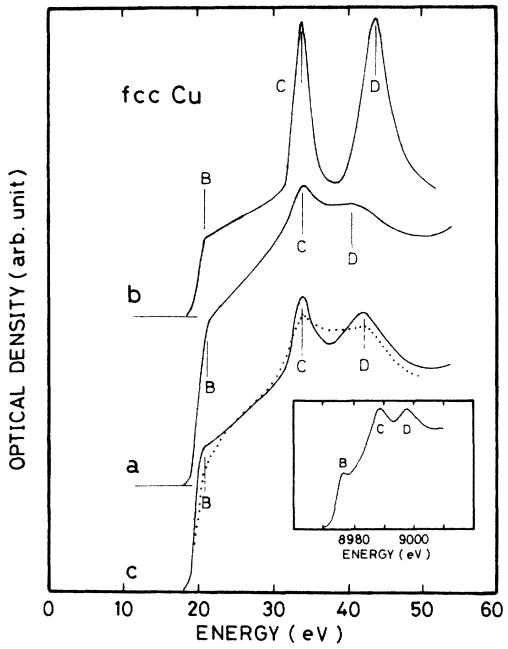

FIG. 6. Calculated K XANES spectra for fcc Cu in the case of $(l_{max},S_{max})=(2,3)$ and the experimental (Ref. 14) one. The curves a and c denote the spectra calculated by the use of the muffin-tin potentials with $r_0=a_0/2$ and $r_0=0.9a_0/2$, respectively, and b is the result obtained from the Chodorow potential (Refs. 15 and 16). The broadening effect is taken into account in curve c, the resultant curve being denoted by the dotted line.

K XANES using the Chodorow potential[15] which is widely used in the band calculation of Cu.[16] The result is shown in curve b in Fig. 6. This shows that the intensities of peaks C and D are strongly enhanced, being much larger than those of the calculated result a in Fig. 6 and the experimental one, but the energy separation between peaks C and D agrees well with the experiment.

D. Potential modification and lifetime broadening

From the above results, XANES is found to be very sensitive to the potential used. This means that the XANES directly reflects the influence of changes in electronic states, for example, core-hole effects, charge-transfer effects in multicomponent materials, etc. Thus, a construction of the potential is a very important problem, especially in materials reacting to the influences of the aforementioned effects.

We have checked the muffin-tin-radius (r_0) dependence of the spectra only for Cr and Cu, due to computational costs. The results for $r_0=0.9a_0/2$ are shown in curve d in Fig. 3 and in curve c in Fig. 6. For Cr, improvement concerning the relative intensity of the B_2 peak has been obtained, and for Cu the overall profile of the calculated

TABLE IV. The peak separation ΔE in eV for fcc Cu (see Fig. 6).

Spectrum	ΔE_{BC}	ΔE_{CD}
a	12.8	6.4
b	13.2	9.8
c	13.2	8.2
Expt.[a]	13.0	9.0

[a]Reference 14.

spectrum approaches the experiment, though the peak near the threshold does not appear in as clear a form as in the experiment.

Now, we present the final spectra, broadened for the best of the various results calculated from Eq. (5). They are shown by the dotted curves for each material in Figs. 3–6. The peak positions remain almost the same as in the unbroadened spectra. In bcc materials, the lifetime broadening effect gives rise to a considerable improvement. Especially, the peak B_2 in Fe is changed in such a manner that the overall profile approaches the experiment. On the other hand, in fcc materials, satisfactory agreement between the calculation and the experiment has been obtained, except that peak B_2 of Ni and shoulder B of Cu have been smeared out.

From the above discussions, the MS theory may not predict peak B in Cu observed at the threshold. We think that its complete explanation lies outside the construction of the appropriate potential, for example, the deviation from the free-electron density of states in the vicinity of the absorption threshold.

V. SUMMARY

We have calculated the K XANES for the $3d$ transition metals Cr, Fe, Ni, and Cu on the basis of MS theory using the muffin-tin potential constructed from the atomic data of Herman and Skillman. The spectra for the XANES in this approach is very sensitive to the potential chosen and it is important to choose suitably the size of the cluster and l_{max}, depending on the nature of the atoms constituting the materials. The results obtained lead us to the conclusion that we can at least predict the number of peaks appearing in the XANES region and their correct peak separations by the MS theory. The advantage of this theory is that it can be applied to disordered systems as well as to ordered ones, and its treatment is easy compared to that based on band-structure calculations whose applicability is restricted to materials having long-range order.

It may be possible to use short-range-order multiple-scattering theory as a tool to analyze the XANES for complicated materials. We are now studying an extension of the present study to the problem of two-component materials.

[1]P. A. Lee and J. B. Pendry, Phys. Rev. B **11**, 2795 (1975).
[2]P. A. Lee, P. H. Citrin, P. Eisenberger, and B. M. Kincaid, Rev. Mod. Phys. **53**, 769 (1981).
[3]F. W. Kutzler, C. R. Natoli, D. K. Misemer, S. Doniach, and K. O. Hodgson, J. Chem. Phys. **73**, 3274 (1980).
[4]P. J. Durham, J. B. Pendry, and C. H. Hodges, Solid State Commun. **38**, 159 (1981).
[5]A. Bianconi, M. Dell'Ariccia, P. J. Durham, and J. B. Pendry, Phys. Rev. B **26**, 6502 (1982).
[6]T. Fujikawa, T. Matsuura, and H. Kuroda, J. Phys. Soc. Jpn. **52**, 905 (1983).
[7]S. Wakoh and Y. Kubo, Jpn. J. Appl. Phys. **17**, 193 (1978).
[8]J. E. Müller, O. Jepsen, and J. W. Wilkins, Solid State Commun. **42**, 365 (1982).
[9]J. E. Müller and J. W. Wilkins, Phys. Rev. B **29**, 4331 (1984).
[10]A. Liebsch, Phys. Rev. B **13**, 544 (1976).
[11]L. F. Mattheiss, Phys. Rev. **133**, B1399 (1964).
[12]F. Herman and S. Skillman, *Atomic Structure Calculations* (Prentice-Hall, Englewood Cliffs, New Jersey, 1963).
[13]O. Kreski-Rahkouen and M. O. Krause, At. Data Nucl. Data Tables **14**, 139 (1974).
[14]L. A. Grunes, Phys. Rev. B **27**, 2111 (1983).
[15]M. I. Chodorow, Phys. Rev. **55**, 675 (1939).
[16]G. A. Burdick, Phys. Rev. **129**, 138 (1963).